Biological Evaluation and Mechanism studies of Novel MK2-RIPK1 Dual Degraders

Jiwon Lee

Department of Medical Science

The Graduate School, Yonsei University

Biological Evaluation and Mechanism studies of Novel MK2-RIPK1 Dual Degraders

Directed by Professor Taebo Sim

The Master's Thesis
submitted to the Department of Medical Science,
the Graduate School of Yonsei University
in partial fulfillment of the requirements for the degree of
Master of Medical Science

Jiwon Lee

December 2023

This certifies that the Master's Thesis of
Jiwon Lee is approved.

Thesis Supervisor : Taebo Sim

Thesis Committee Member#1 : Hyunseok Kim

Thesis Committee Member#2 : Hwangeun Choi

The Graduate School
Yonsei University

December 2023

<TABLE OF CONTENTS>

LIST OF FIGURES

LIST OF TABLES

ABSTRACT

Biological Evaluation and Mechanism studies of Novel MK2-RIPK1 Dual Degraders

Jiwon Lee

Department of Medical Science
The Graduate School, Yonsei University

(Directed by Professor Taebo Sim)

Kinase is an important enzyme that plays a key role in multiple cell signaling pathways and regulates various cellular functions, such as the cell cycle, proliferation, growth, differentiation, metabolism, and inflammation. Kinase dysfunction is implicated in several human diseases, including oncological, immune, and neurological conditions. Because of these reasons, many drugs that inhibit kinases have been developed. But these kinds of drugs still have several issues for development, including drug resistance, low selectivity, and undruggable targets.

Recently, a new approach called Proteolysis-Targeting Chimera (PROTAC) has emerged. This technology can address the limitations of current inhibitors. It consists of three components: a protein of interest, a recognizing E3 ligase, and a linker. With these structural features, PROTAC utilizes a targeted protein degradation (TPD) technology that leverages the intracellular ubiquitin proteasome system (UPS). With this approach, our previous research thoroughly analyzed the chemo-proteomics profiling of degraders based on GNF-7. Through previous research, we have found that VHL-PROTAC, with GNF-7 as a warhead, has the ability to selectively degrade MK2 and RIPK1.

In this study, we designed and synthesized 16 derivatives having GNF-7 moiety as warhead. A structure activity relationship (SAR) study led to the discovery of MK2 selective degrader **(30b)** as chemical tool compound. **30b** possessing trifluoroexthoxy pyridine warhead has excellent degradation selectivity toward MK2 (DC_{50} for MK2 = 0.005 ± 0.001 μM and RIPK1 = >2.5 μM). Furthermore, we revealed that **30b** depleted the target kinase protein in a dose-, time-, VHL- and UPS- dependent manner by performing various biological evaluations. We also showed that **30b** directly binds to p38alpha and indirectly degrades MK2. We presented a study using molecular modeling on the ternary complex model of **30b**, involving the p38alpha-MK2 heterodimer and the von Hippel-Lindau (VHL) Cullin RING E3 ligase. Moreover, **30b** has moderate *in vivo* efficacy and degrades MK2 excellently in MOLT-4 mouse xenograft model.

MK2 is a crucial kinase in the inflammatory signaling pathway and tumor progression by regulating RBPs (RNA binding proteins). To date, several inhibitors targeting MK2 have been developed. Most MK2 inhibitors, except ATI450, still present hurdles in clinical development. Recently, the MK2 degradation approach has emerged as an effective strategy for inhibiting MK2, but the degrader has been poorly studied. By considering the results of this study as a whole, we gain insight into the development of a novel MK2 selective degrader, along with MK2-RIPK1 dual degraders. And this study supports further investigation of **30b** as an effective treatment for inflammatory diseases and for cancer therapy.

Key words : kinase, targeted protein degradation, proteolysis-targeting chimera, design, synthesis, degradation mechanism, MK2-RIPK1 dual degrader, MK2 selective degrader

Biological Evaluation and Mechanism studies of Novel MK2-RIPK1 Dual Degraders

Jiwon Lee

Department of Medical Science
The Graduate School, Yonsei University

(Directed by Professor Taebo Sim)

I. INTRODUCTION

The human genome encodes more than 500 protein kinases, including tyrosine kinases and lipid kinases [1, 2]. These protein kinases catalyze the transfer of a γ-phosphate group from ATP to a substrate protein and initiate signal transduction through the phosphate [3]. Protein phosphorylation by kinases triggers cell signaling pathways and regulates cellular functions such as the cell cycle, proliferation, apoptosis, differentiation, metabolism, and inflammation [4]. Since these molecules play a major role in several intracellular functions, kinase dysfunction is related to human disorders including oncogenesis, immune, and neurological diseases. Most protein kinases have the potential to be therapeutic enzymes and serve as drug targets [5]. Over the past few years, there has been development and exploration of small kinase inhibitors directly targeting protein kinases, which has resulted in FDA-approved kinase inhibitors [6]. However, molecularly targeted therapies like kinase inhibitors still remain a number of issues for development [7]. Many kinase inhibitors rely on the occupancy-driven mechanism to achieve high target occupancy and drug efficacy, often requiring high drug concentrations. This strategy induces binding to off-targets and results in side effects [8, 9]. And there is also low

selectivity and drug resistance [10]. Recently, a technology called proteolysis-targeting chimera (PROTAC) has emerged as one of the targeted protein degradation (TPD) method. This technology shows promise as a new approach to therapy from an innovative perspective in drug discovery [11]. Structurally, it is a hetero-bifunctional molecule that conjugate target protein binding moiety (warhead) to an E3 ligase ligand by intervening chemical linker. This design leads to the formation of a ternary complex with the target protein and E3 ligases like VHL and CRBN, activating the intracellular ubiquitin-proteasome system (UPS). Subsequently, PROTAC causes the target protein to undergo poly-ubiquitination and degradation completely [12] **(Figure 1)**. Consequently, this event-driven strategy has the advantage of overcoming the limitations of the mentioned kinase inhibitors by degrading the target kinases.

In this study, we discovered novel MK2 degrader (**30b**) incorporating PROTAC technology derived from MK2-RIPK1 dual degraders Before starting this study, in our previous research [13], we conducted chemo-proteomics on several degrades with GNF-7, a multi-targeted inhibitor as warhead. Through this global proteomics profiling, it showed that VHL-PROTAC with GNF-7 is more capable of significantly degrading MAPKAPK2 (MK2) and Receptor-interacting serine / threonine-protein kinase 1 (RIPK1) protein kinases than CRBN-PROTAC **(Figure 2)**. These previously founding data provided clues for developing degraders for MK2 and RIPK1. Sixteen different derivatives were synthesized and designed. Afterwards, a structure activity relationship (SAR) study was performed by measuring western blot-based degradation activity to derive the lead compound. In SAR study, first we demonstrated **18e**, MK2-RIPK1 dual degrader possessing higher degradation potency against both MK2 and RIPK1. (DC_{50} for MK2 = 0.003 ± 0.001, RIPK1 = 0.017 ± 0.001 μM). And then by modifying the warhead with bulky group, trifluoreoethoxy pyridine, we displayed **30b**, MK2 selective degraders, which has higher degradation selectivity for MK2 (DC_{50} for MK2 = 0.005 ± 0.001 μM and RIPK1 = > 2.5 μM).

First, we conducted several assays including rescue experiments, the CRISPR Cas9 VHL knockout system, CETSA, and the VHL target engagement assay to uncover the degradation mechanism of **30b**. As a result, we found that **30b** significantly reduces MK2 in the ubiquitin-proteasome system by anchoring VHL. Furthermore, while there was excellent enzymatic activity against p38alpha with an IC_{50} of 2.48 nM, but no obvious enzymatic activity against MK2. Hence, we showed that **30b** is an MK2 indirect degrader. According to previous research [14, 15, 16,] MK2 is a direct downstream substrate of p38alpha. p38alpha forms a heterodimer complex with MK2. Through molecular docking study, we revealed that **30b** could interact the p38alpha-MK2 heterodimer and form a ternary complex model with VHL. Following the theoretical background and docking study, we believed that the degradation of MK2 is related to p38alpha. We observed that **30b** causes the formation of a ternary complex (VHL: degrader: p38alpha). Subsequently, p38alpha was degraded by **30b** in a dose- and time-dependent manner. From these results, we discovered that the degradation of MK2 is associated with p38alpha. Lastly, we conducted *in vivo* degradation investigation of **30b** on MOLT-4 mouse xenograft model. And we found that **30b** induce degradation for MK2 (% of degradation = 89%) completely.

MK2 plays essential role in inflammatory response. Activated MK2, released form the MK2-p38alpha heterodimer complex, regulates the mRNA stability and expression of pro-inflammatory cytokines and proto-oncogenes [17, 18, 19, 20]. Therefore, many MK2 inhibitors have been developed as a promising therapeutic agent for inflammatory diseases and cancer [21, 22, 23]. Despite efforts to inhibit MK2 activity, there are still limitations to contend with, including poor solubility, low cell permeability, and insufficient selectivity and low biochemical efficiency (BE) value [24]. To date, ATI450 is the only compound that has entered phase 2 clinical trials [25]. Therefore, there is need to study more effectively inhibition MK2. Degradation of MK2 strategy is emerging as another MK2 inhibition approach as a new modality [26]. And so far, no MK2 selective degrader by harnessing PROTAC technology have been reported. Our

representative compound, **30b**, is an MK2 indirect degrader that harnesses PROTAC technology. It is expected to overcome the limitations of current MK2 inhibitors and also have effective anti-inflammatory effects. In this thesis, we identified a selective and potent MK2 degrader, **30b**, which exhibits excellent degradation activity against MK2. The mechanism for **30b** was demonstrated through *in vitro* and *in vivo* studies. Overall, our results offer new insights into the design of MK2 degrader and provide valuable resources for further research and development of treatments for inflammatory diseases such as rheumatoid arthritis (RA), psoriasis, and inflammatory bowel disease (IBD), as well as oncological diseases.

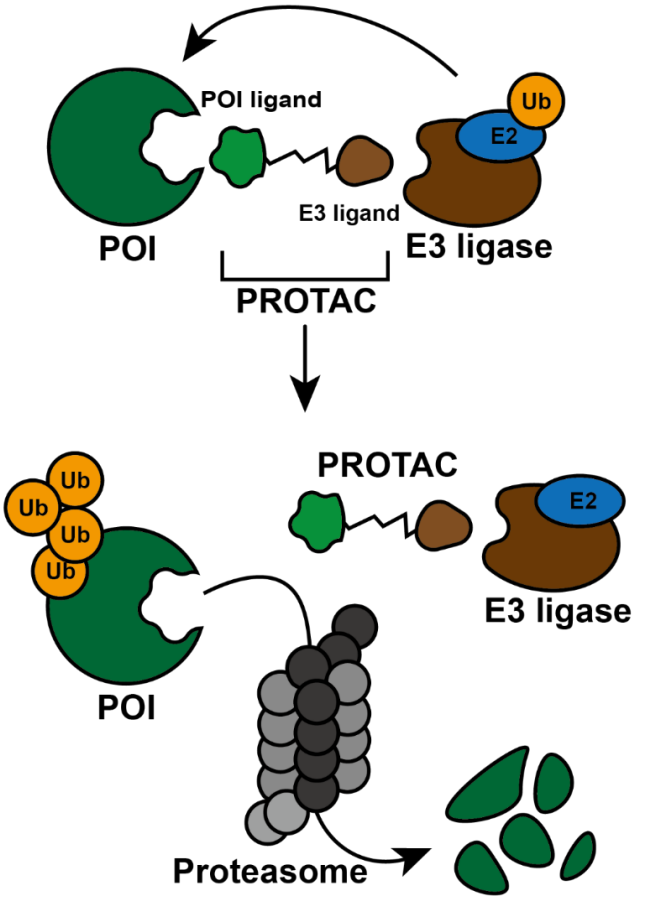

Figure 1. Scheme of proteolysis-targeting chimera (PROTAC) degradation mechanism.

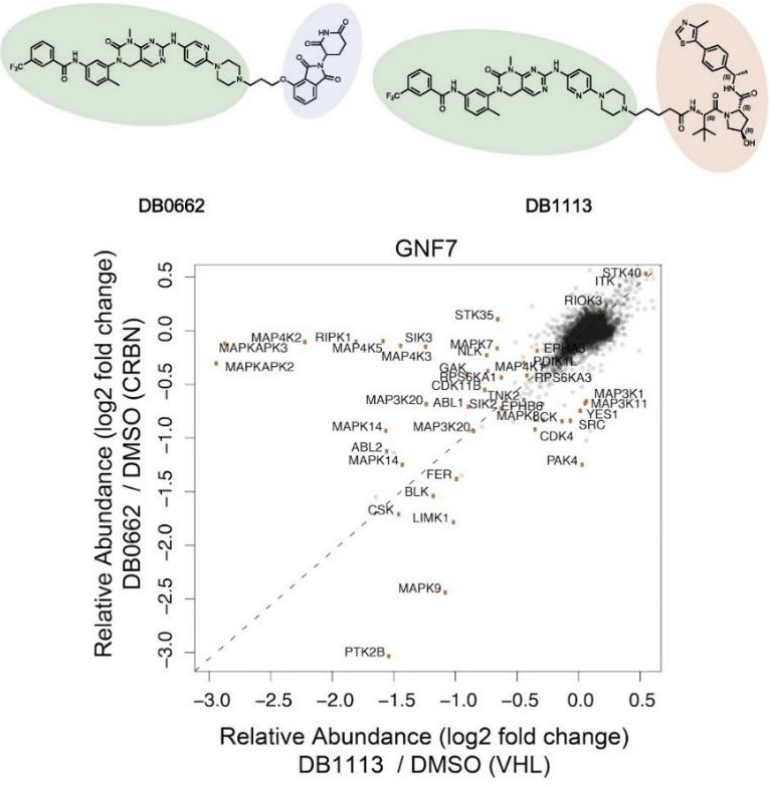

Figure 2. Global proteomics profiling of DB1113 and DB0662 [13].

II. MATERIALS AND METHODS

1. Chemical synthesis

All the derivatives were provided by our lab and made up as a 10 mM stock solution in DMSO by Minjoo Ko.

2. Cell culture

MOLT-4 and 293T cell lines were obtained from the American Type Culture Collection (ATCC, USA). BRD-GFPΩmCherry HELA cells have been established in our laboratory. MOLT-4 cells were cultured in RPMI1640 (Welgene, Seoul, Korea), while 293T and BRD-GFPΩmCherry HELA cells were incubated in DMEM (Welgene, Seoul, Korea). All of these culture media contained 20% FBS (Welgene, Seoul, Korea) and 1% penicillin/streptomycin (Welgene, Seoul, Korea). The cells were placed in a humid environment with 5% CO_2 at 37 ℃. The cultured cells were verified to be negative for mycoplasma using the *BioMycoX*® Mycoplasma PCR Detection Kit (Cell Safe D-100, Korea).

3. Anti-proliferation assay (Celltiter glo)

A total of $3x10^3$ cells were placed into every well of a 96-well plate. After seeding, 3-fold serially diluted compounds in DMSO were treated to the cells. After 72 h incubation at 37 ℃, Celltiter-glo (G7572, Promega, USA) 30 μL (working solution) was added to each well. The 96 well plate reader, (Envision) was utilized to detect the luminescence signal produced by the viable cells. Fitted does-dependent curves and GI_{50} values were obtained by Graphpad Prism 8.0.2 software. All experiments were conducted in duplicate with three independent assays.

4. Western blot

The Cells were plated at the density of $1x10^6$ cells/well in a 60 mm dish. Following seeding, the cells were exposed to the compounds for the designated duration at a temperature of 37 ℃ in a 5% CO_2 environment. Cells were washed twice with cold PBS. Thereafter, cells were subjected to lysis in a Triton X-100 buffer (50 mM Tris-HCl pH7.5, 1% Triton X-100, 1 mM EDTA, 150 mM NaCl) containing 1× protease inhibitor cocktail (Roche) and 1x phosphatase inhibitor (Roche). Lysate was then cleared at 13000 rpm for 20 min at 4 ℃. Protein concentrations of the supernatants were then quantified using a Pierce BCA Protein Assay. The equal amount of lysate was separated by SDS-PAGE gel and transferred to NC membrane (Millipore, #IPVH00010). The membranes were then blocked in 5% skim milk in TBS-T. The membrane was probed with uniformly diluted primary antibody at 1:1000 (v/v) in TBS-T. After incubating with secondary antibodies at 1:10000 (v/v) for 1 h at room temperature, ECL solution was treated and the immune reactive proteins were imaged by ImageQuantTMLAS4000 (GE Healthcare, USA). Membranes. All primary antibody used for GAPDH (#5174), MAPKAPK-2 (#3042), RIPK1 (#3493), p38alpha (#8690) were purchased from Cell Signaling Technologies (Massachusetts, USA). beta - Actin (sc-47778) was obtained from Santa Cruz. And HRP-conjugated goat anti-rabbit secondary antibody (SA002-500) were purchased from Gendepot (Katy, TX, USA).

5. RNA isolation and Reverse Transcription PCR (RT-PCR)

MOLT-4 cells were seeded at 1 × 10^6 cells/ml, and then were treated with either DMSO or compound **30b**. TRIzol reagent (Invitrogen, 15596-026) was added to each sample in a volume of 1 mL to lyse the cells. 200 μL of Chloroform was added to each sample, and then the samples were thoroughly mixed by vortexing. After that, they were centrifuged at 13000 rpm for 15 min at 4 ℃. Total RNA was precipitated from the aqueous phase by adding 500 μL of isopropanol then centrifuging at 13000 rpm for 10 min at 4 ℃. The RNA pellet was rinsed twice with 75% ethanol and then allowed to dry in the open air for 15 min. After that, the RNA was dissolved in 20 μL of DEPC-treated water and subjected to Nanodrop analysis to determine its concentration and purity. Complementary DNA (cDNA) was synthesized using 2 μg of total RNA per condition, following the protocol provided by manufacturer (Applied PROMEGA, M1701). RT-PCR was then performed using SafeDryTaq premix (LTP-480) and analyzed using a thermocycler. Two independent trials were carried out to analyze the RT-PCR samples. Normalization was performed using GAPDH. The primers used in this study are listed in **Table 1**, and PCR conditions are described as follows in **Table 2**.

6. CHX chase assay

MOLT-4 cells were plated at a density of 1x10^6 cells per well in a 60 mm dish. CHX was initially administered to cells at a concentration of 100 μg/ml for 60 min before the subsequent addition of either DMSO or degrader (**30b**). At the specified time intervals, the cells were promptly placed on ice, washed with 1xPBS, lysed, and then boiled.

7. Cellular Thermal Shift assay (CETSA)

$10x10^6$ cells/ml of MOLT-4 cells were seeded in an E-tube. Cells were pre-treated with MG132 at a concentration of 1 μM for a duration of 1 h. Following this, they were treated with DMSO and degraders at a concentration of 1 μM for 10 min at a temperature of 37 ℃ in an atmosphere containing 5% CO2. In total, $2x10^7$ MOLT-4 cells ($1x10^6$ cells per condition) were harvested and suspended in ice-cold 1x PBS. Then, they were lysed by three cycles of liquid nitrogen snap freeze. The sample was subjected to a 50% thaw in a water bath at room temperature, followed by an additional 50% thaw at 4 ℃. The lysate was vortexed briefly after every freeze-thaw cycle to ensure even thawing. The lysate was cleared for 20 min by centrifugation (13000 rpm at 4 ℃). The soluble fraction was then divided into 8 PCR tubes, with each tube containing 100 μL. Each tube was heated at the indicated temperature for 10 min. The samples were centrifuged at 13000 rpm for 20 min at 4 ℃. The resulting supernatant, which represents the soluble fraction, was then analyzed using SDS-PAGE and immunoblotting to detect VHL and beta-actin (used as a negative control).

8. Target engagement assay

A. Flow cytometry (FACS)

BRD-GFPΩmCherry HELA cells were plated in a 12 well plate at $1x10^6$ cells/ml and incubated overnight. After incubating the cells, MZ1 and PROTACs were applied to them for 4 h at 37 ℃ in a 5% CO_2 atmosphere. Total cells were harvested using a trypsin-EDTA solution, collected by centrifugation, washed with PBS, and resuspended in PBS. Fluorescence intensity was analyzed by using a flow cytometer (BD Canto II, BD biosciences, USA).

B. HCS imaging

BRD-GFPΩmCherry HELA cells were seeded at a density of $4x10^4$ cells/ml on a 96 well black plate. After cell adhesion, MZ1 and PROTACs were treated for 4 h at 37 ℃ in a 5% CO_2 atmosphere. The plates were imaged automatically using Operetta (PerkinElmer). All experiments were performed in duplicate.

9. CRISPR-Cas9 system mediated VHL knockout 293T cell line

The sgRNA oligos, with their sequence information listed in **Table 3**, were designed using the CRISPR sgRNA Database on the Sanjana lab website. These oligos were cloned into a pAWP28 vector (#73850) and then subcloned into a PTK799 vector. The lentiviral expression vector containing Cas9, known as LentiCas9-Blast construct, was obtained from Addgene (#52962). Initially, a Cas9 293T cell line construct was generated by infecting the cells with a virus. And then, to create VHL knockout Cas9 293T stable cells, we conducted viral infection and subsequently selected cells using blasticidin at a concentration of 15 μg/ml for 3 days.

10. DNA cloning

pNLF1-N [CMV/Hygro] Vector (N135A, Promega), pHTC HaloTag® CMV-neo Vector (G7711, Promega) HaloTag® -VHL Fusion Vector (N273A, Promega) and pCDNA3 Flag p38 alpha (20351, Addgene) were purchased. Nluc-VHL (C-terminal) and p38alpha-Halo (C-terminal) were generated using the constructs described above. Inserts containing restriction sites for VHL and p38alpha were obtained through PCR. And then DNA fragments were cut by restriction enzyme sites. The ligation mix kit (6023.Takara) was used to ligate the Inserts and Vectors together. DH5alpha transformation and colony selection were performed. And both VHL tagged Nluc (N-terminal) and p38alpha tagged Halo (C-terminal) have been obtained and completely validated by sequencing (Macrogen, Seoul, Korea).

11. NanoBRET ternary complex assay

p38alpha, tagged with Halo at the C-terminal, and VHL, tagged with Nluc at the N-terminal, are co-transfected into 293T cell lines. After 24 h, the 293T cells that were co-transfected were transferred to a 96-well white plate (30196, SPL Life Sciences) at a density of 4.4×10^4 cells per well using Opti-MEM™ I Reduced Serum Medium, without phenol red (31985070, Gibco™) + 4% FBS adding HaloTag® NanoBRET™ 618 Ligand (G9801, Promega). After an overnight incubation, MG132 and Degraders were treated and added with a 1X solution of NanoBRET™ Nano-Glo® Substrate (N1571, Promega) 25 µL to cells. After that, luminescence emission (460 nm) and fluorescence emission (618 nm) were measured by Envision (Perkin Elmer). mBU was calculated using the following formula. $618nm_{Em} / 460nm_{Em}$ = BU x 1,000 = mBU

12. MOLT-4 mouse xenograft model

All animal experiments conducted in facilities accredited by the AAALAC and authorized by the Yonsei ABMRC Animal Facilities and Use Committee. The MOLT-4 cells were rinsed twice with RPMI1640 (without FBS and penicillin/streptomycin) to effectively remove FBS and antibiotics. The right flank of 5 week-old female Balb/c nude mice (Orient Bio, Inc., Seoul, Korea) was injected subcutaneously with a mixture of MOLT-4 cells ($5x10^6$ cells/100 μL) and Matrigel (#354234, Corning) in a 1:1 ratio. When the average of tumor volume was approximately 100 mm^3, the mice tumors were randomly arranged into 2 cohorts (n = 5 per cohort): vehicle, 10 mg/kg **30b**. The compound was formulated in vehicle. The vehicle substances are as follows: 5% NMP and 95% 20% RH40. Mice were given a vehicle and a dose of 10 mg/kg **30b** via intravenous injection twice a week. Tumor volume and body weight were monitored once every 2 days. The formula for tumor volume calculation in this thesis is 1/2 [longest length x (shortest length)]^2 mm^3.

13. *in vivo* western blot analysis

The tumor tissues were dissected from the mice, sliced, and weighed. One bead was added per Sample Tube RB (round bottom shape sample tube) (990381, QIAGEN, Germany) And sliced tumor tissues were transferred to a round tube containing beads. After that T-PER™ Tissue Protein Extraction Reagent was added according to the weight of tumor tissue (e.g. 10 mg/100 μL). The tumor tissues were homogenized by using the TissueLyser II (QIAGEN, Germany) for 3 min at 30 HZ. The next steps for obtaining the lysate and producing the sample are identical to the western blot procedure described above.

14. Molecular docking study

Docking study was performed by Minjoo Ko.

15. Statistical analysis

The results were visualized and analyzed using Prism software 8.0.2 (GraphPad Software, USA). Numerical data is typically presented as mean ± standard deviation (SD). An examination of the "Student's" t-test was conducted to evaluate the statistical significance. *p* values below 0.05 were deemed statistically significant and were noted in the figure legends.

Table 1. RT-PCR primers

Gene Name	5' → 3'	Product size
MK2-F	TCATGAAGCATCGGTGAG	165 bp
MK2-R	TCAAAGAGTTGTGGCTGGTG	
GAPDH-F	GGATTTGGTCGTATTGGG	205 bp
GAPDH-R	GGAAGATGGTGATGGGATT	

Table 2. RT-PCR conditions

Step	Temperature	Time	Cycle
Initial denaturation	95 ℃	5 min	1 cycle
Denaturation	95 ℃	30 sec	
Annealing	60 ℃	30 sec	40 cycles
Extension	72 ℃	30 sec	
Final elongation	72 ℃	5 min	1 cycle
Cooling	4 ℃	Unlimited time	1 cycle

Table 3. Oligo sequences of sgVHL

Target gene	Oligo duplex / sg VHL (5'→ 3')
VHL	CACCGCATACGGGCAGCACGACGCG
	AAACCGCGTCGTGCTGCCCGTATGC

III. RESULTS

1. SAR study leads 30b as a selective and potent MK2 degrader

As mentioned in the introduction, global proteomics profiling has revealed that DB0662 (a CRBN-PROTAC with GNF-7) and DB1113 (a VHL-PROTAC with GNF-7) exhibit distinct selectivity in degrading MK2 and RIPK1 proteins. In **Figure 2**, it is evident that the VHL binder DB1113 effectively degrades MK2 and RIPK1, compared to the CRBN binder DB0662, in MOLT-4 cells. Based on data from previous studies, we designed and synthesized sixteen degraders based on GNF-7. We modified the E3 ligase binder, linker length and composition, as well as the warhead to optimize the degraders for MK2 and RIPK1.

To evaluate the degradation activity of each compound, we calculated the half-maximal degradation concentration (DC_{50}) values on MOLT-4 cells and conducted a comparative analysis. The DC_{50} represents the protein concentration at which 50% degradation occurs, corresponding to half-maximal degradation. Using western blot analysis, we determined the DC_{50} values of MOLT-4 cells by performing a series of 1/3 dilutions for each compound. The results shown are the mean of two independent experiments performed for 4 h.

The first series of derivatives (**15a-15b**) was designed by connecting CRBN to methyl linkers of various lengths. As shown in **Table 4** and **Figure 3A-3K**, both **15a** and **15b** did not show any degradation effect, even when the length of the linker was modified. The second series of derivatives (**18a-18g**) was prepared by attaching VHL to various linker lengths and compositions. Conversely, some of the compounds (**18a-18b**, **18e-18g**) showed excellent degradation activity against MK2 and RIPK1. **18a** and **18b** presented comparable DC_{50} values to DB1113, but compounds with relatively long linkers, **18c** and **18d**, showed lower or no degradation activity compared to compounds with shorter

linkers (**18a-18b**). These results indicate that a longer linker is not favorable for degradation on MOLT-4. Moreover, derivatives introducing oxygen atom (**18e-18g**) showed that a similar pattern were observed in the difference in degradation as the linker length increases. Among these compounds, compound **18e** demonstrated significantly enhanced degradation for MK2 and RIPK1, approximately 2 to 3-fold higher compared to compound **18b**, which has the same linker length. Collectively, we found that **18e** is the optimal compound for dual degradation of MK2 and RIPK1. **18e** was observed to reduce the degradation activity of MK2 and RIPK1 to DC_{50} values of 0.003 ± 0.001, 0.017 ± 0.001 μM, respectively.

Additionally, we synthesized a third series of derivatives to optimize the warhead. These derivatives include bulky functional groups such as methoxy, trifluoroethoxy pyridine, and dichloro benzene (**Table 5**). **Table 5** and **Figure 4A-4G** showed that the modified compounds in the warhead resulted in an improved selectivity for MK2 degradation. **27a** (DC_{50} of MK2 = 0.014 ± 0.000 μM, RIPK1= 0.588 ± 0.137 μM) showed 42-fold selectivity for MK2 compared to **27b** (DC_{50} of MK2 = 0.024 ± 0.001 μM, RIPK1 = 1.029 ± 0.168 μM). Additionally, **27b**, which has trifluoroethoxy pyridine as a warhead, exhibited 80-fold greater selectivity for MK2 degradation over RIPK1. Derivatives with modified linker composition to alkyl chain (**30b**, **37b**), while maintaining the same warhead, binder, and number of atoms, exhibited 10 to 20-fold higher selectivity compared to **27b** and **37a**. Compound **42** demonstrates comparable selectivity to other compounds in degrading MK2 when combined with dichlorobenzene. According to the results, we have shown that the addition of a bulky group with an alkyl linker enhances the selectivity for MK2 degradation. Herein, we selected **30b** as a novel MK2 selective degrader. This is because it not only has a warhead with bulky group compared to other derivatives, but also has excellent potency of selectivity for MK2 compared to RIPK1.

Taken together, in this SAR study, we synthesized several MK2-RIPK1 dual degraders (**18a-18b**, **18e-18g**). And through warhead modification, we finally found the MK2 selective degraders. Among these derivatives, we selected **30b** as a representative compound which has selectively reduced MK2 without affecting RIPK1.

Table 4. Degradation activity against MK2 and RIPK1 of the first and second series derivatives

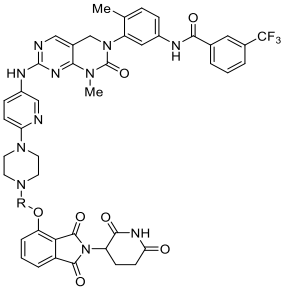

15a-b

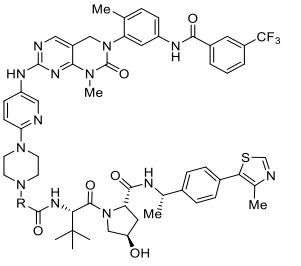

18a-g

Compound	R	DC_{50} in MOLT-4 (μM)[1]	
		MK2	RIPK1
DB0662	-	> 2.5	> 2.5
DB1113	-	0.002 ± 0.000	0.044 ± 0.010
15a	C_5H_{10}	> 2.5	> 2.5
15b	$C_{11}H_{22}$	> 2.5	> 2.5
18a	C_2H_4	0.039 ± 0.003	0.022 ± 0.005
18b	C_6H_{12}	0.008 ± 0.002	0.027 ± 0.001
18c	C_8H_{16}	> 2.5	0.052 ± 0.006
18d	$C_{10}H_{20}$	> 2.5	> 2.5
18e	$C_2H_4OCH_2$	0.003 ± 0.001	0.017 ± 0.001
18f	$C_2H_4OC_2H_4$	0.010 ± 0.002	0.027 ± 0.008
18g	$C_2H_4OC_2H_4OC_2H_4$	0.074 ± 0.004	0.107 ± 0.015

[1] The term "DC_{50}" refers to the concentration at which a compound causes 50% protein degradation.

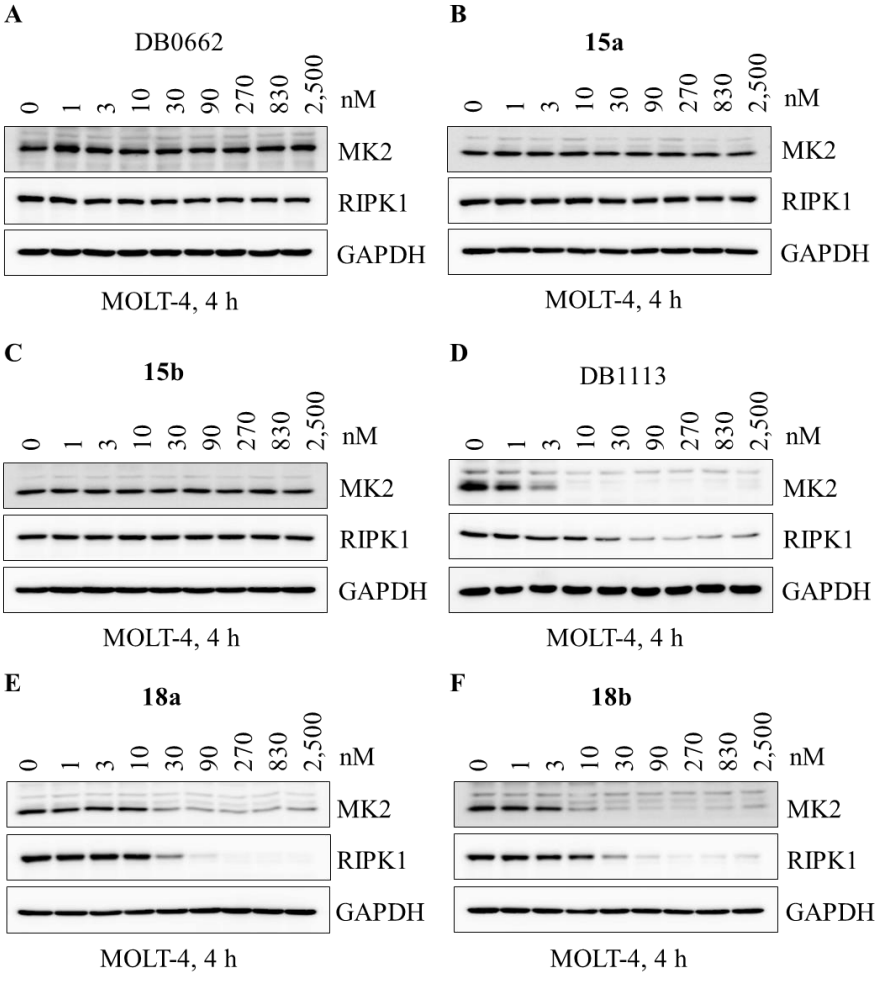

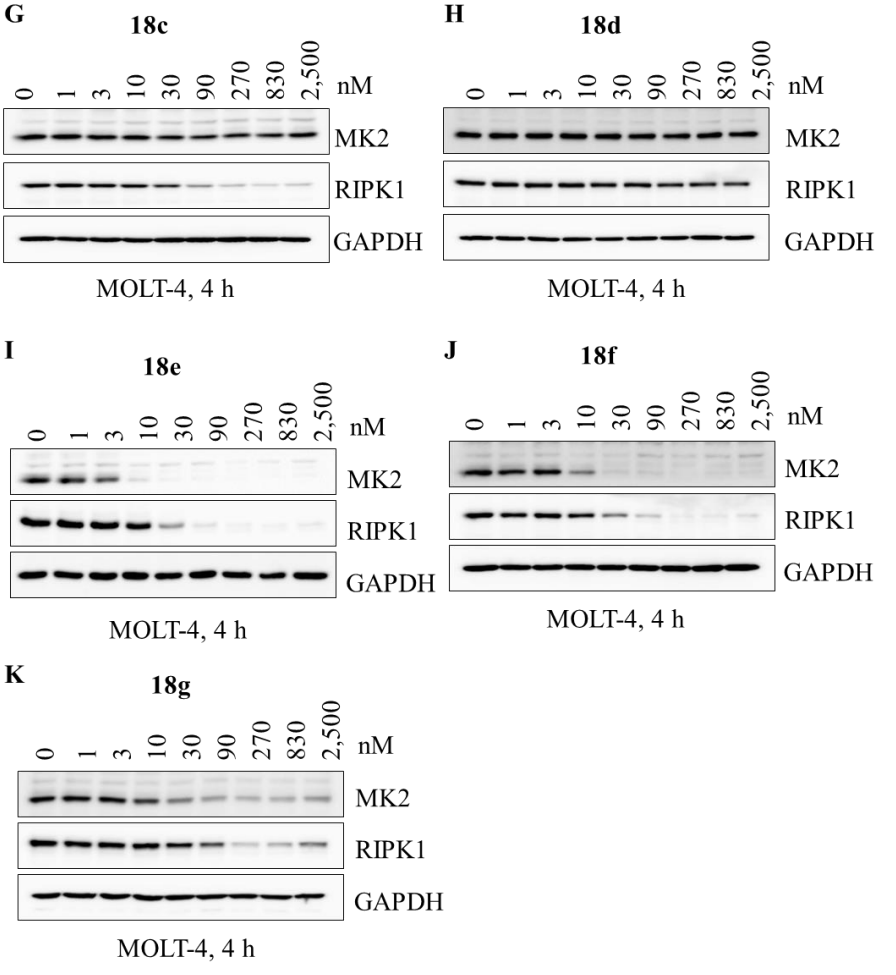

Figure 3. Degradation effects on MK2 and RIPK1 of DB0662, DB1113, and 18a-18g. (A-K) Western blot analysis of MK2 and RIPK1 in MOLT-4 after treatment with different concentration (1/3 serial dilution, Max 2.5 μM) for 4 h. Glyceraldehyde-3-phosphate dehydrogenase (GAPDH) was selected as a loading control.

Table 5. Degradation activity against MK2 and RIPK1 of the third series derivatives

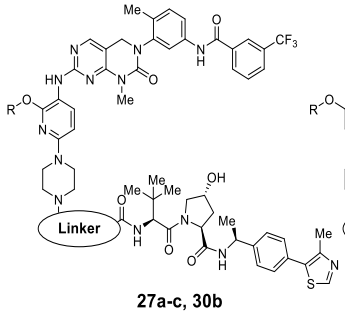

27a-c, 30b

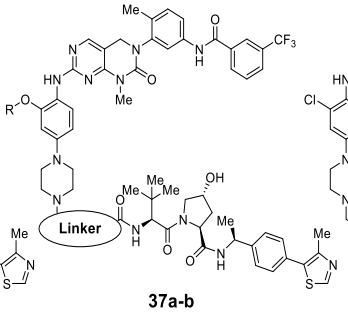

37a-b

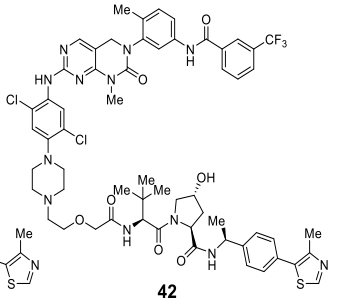

42

compound	R	Linker	DC_{50} in MOLT-4 (μM)[1]	
			MK2	RIPK1
27a	CH_3	$C_2H_4OCH_2$	0.014 ± 0.000	0.588 ± 0.137
27b	CH_2CF_3	$C_2H_4OCH_2$	0.024 ± 0.001	1.029 ± 0.168
27c	$CH_2(CH_3)_2$	$C_2H_4OCH_2$	0.057 ± 0.022	>2.5
30b	CH_2CF_3	C_4H_8	0.005 ± 0.001	> 2.5
37a	CH_3	$C_2H_4OCH_2$	0.015 ± 0.005	0.135 ± 0.046
37b	CH_3	C_4H_8	0.009 ± 0.002	> 2.5
42	-	$C_2H_4OCH_2$	0.015 ± 0.004	1.342 ± 0.059

[1] The term "DC_{50}" refers to the concentration at which a compound causes 50% protein degradation.

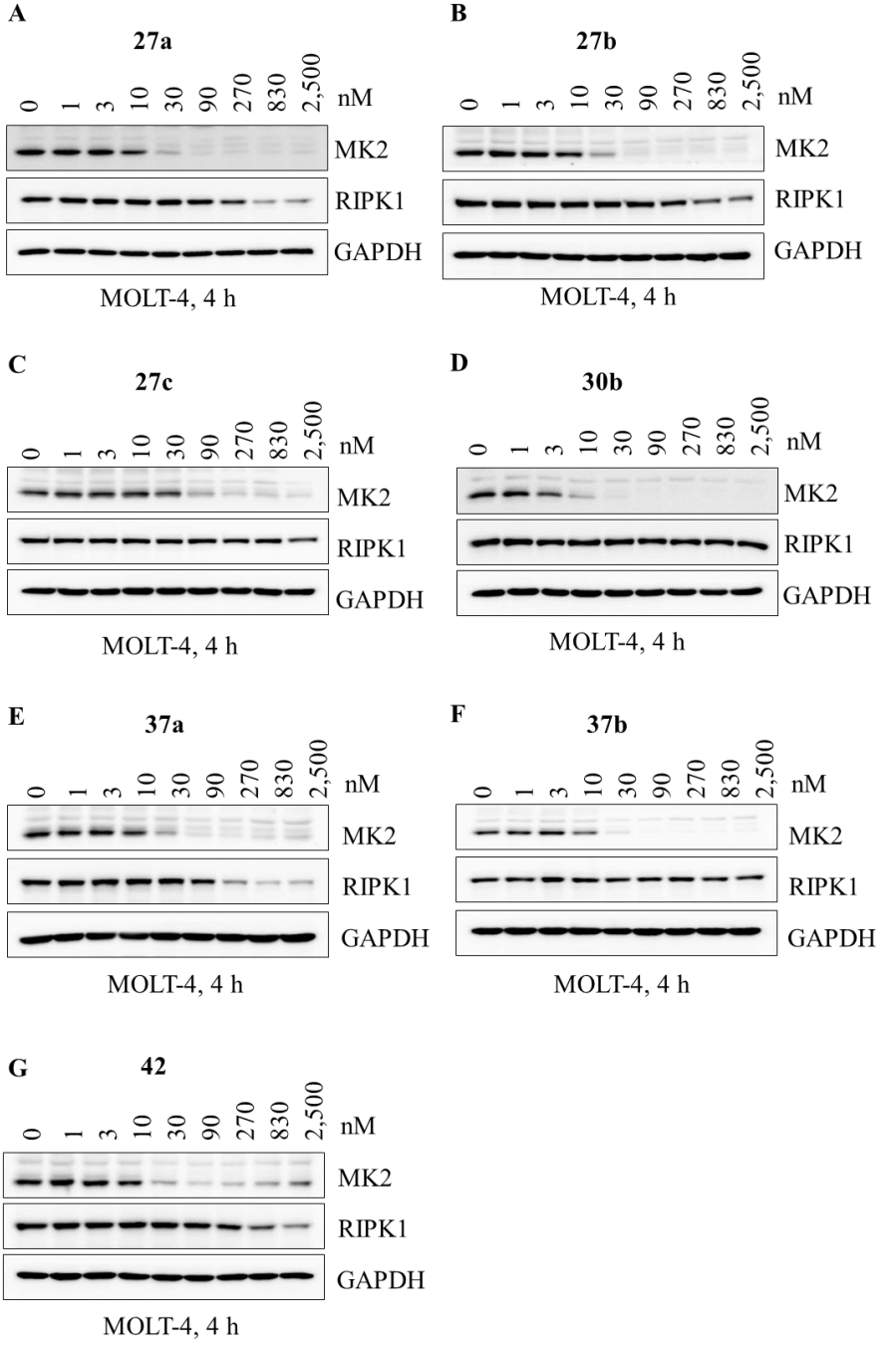

Figure 4. Degradation effects on MK2 and RIPK1 of 27a-27c, 30b, 37a-37b, 42. (A-G) Western blot analysis of MK2 and RIPK1 in MOLT-4 after treatment with different concentration (1/3 serial dilution, Max 2.5 μM) for 4 h. Glyceraldehyde-3-phosphate dehydrogenase (GAPDH) was selected as a loading control.

2. 30b reduces the level of MK2 protein in a UPS-dependent manner

First, MOLT-4 cells were pretreated with cycloheximide (CHX) 100 μg/ml (known as a protein synthesis blocker) for 1 h to block the protein synthesis system. And were treated with **30b** at a concentration of 1 μM for 0 to 24 h, sampling at different time points to monitor the effects of **30b** on MK2's stability in the presence of CHX. As shown in the **Figure 5A**, the group treated with CHX and **30b** demonstrated a significant degradation of MK2 over time compared to the group treated with CHX only. These results indicate that the decrease in MK2 protein level is caused by **30b**, rather than by inhibition of protein synthesis. Additionally, we collected MOLT-4 cells treated with **30b** and conducted RT-PCR. **Figure 5B** showed that **30b** could not downregulate MK2 at the transcriptional level when MK2 was degraded. The above results show that the reduction in target kinases by **30b** occurred at the intracellular protein level, rather than being regulated by mRNA expression.

In eukaryotic cells, there are two main degradation pathways: proteasomes and lysosomes [27]. Therefore, we conducted a rescue experiment to gain insight into the degradation mechanism of MK2 of **30b**. MOLT-4 cells were first treated with 3 μM MG132 (a proteasome inhibitor), 3 μM Epoxomicin (another proteasome inhibitor), 3 μM MLN4924 (an inhibitor of NEDD8-activating enzyme) for 1 h, and **30b** (1 μM) for 4 h. These western blot analysis results indicate that MK2 was completely rescued (**Figure 5C**). We additionally combined treated cells with **30b** and 200 nM bafilomycin A1 (BaFA1, autophagolysosome inhibitor) to prove that the cells were not degraded by lysosomes (**Figure 5D**). As a result, we found that MK2 was degraded even though it blocked the lysosomal degradation system. These data provided that **30b** is indeed responsible for the degradation of MK2 through the ubiquitin-proteasome system (UPS).

In addition, we conducted a competition experiment to demonstrate that the degradation of MK2 is mediated by a KMJ059101 warhead. We discovered that the MK2 fully recovered with the co-treatment of **30b** and the warhead. This data indicates that the degradation of MK2 only happens when the warhead of the **30b** degrader is present (**Figure 5E**).

To verify that the degradation of MK2 is linked to VHL, Minjoo Ko synthesized a negative degrader (KMJ063749) that does not have the ability to bind VHL. After treating MOLT-4 cells with various concentrations of **30b** and negative degrader, the degradation of MK2 was compared. **Figure 5F** revealed that the negative degrader prevented degradation effects on MK2. Next, we established VHL knockout 293T cell lines using CRISPR-Cas9 system. As a result, the degradation effect of MK2 is blocked in VHL knockout 293T cell lines (**Figure 5G**). All these data indicate that MK2 is induced into the intracellular proteasome system by the PROTAC-based degrader **30b.**

A

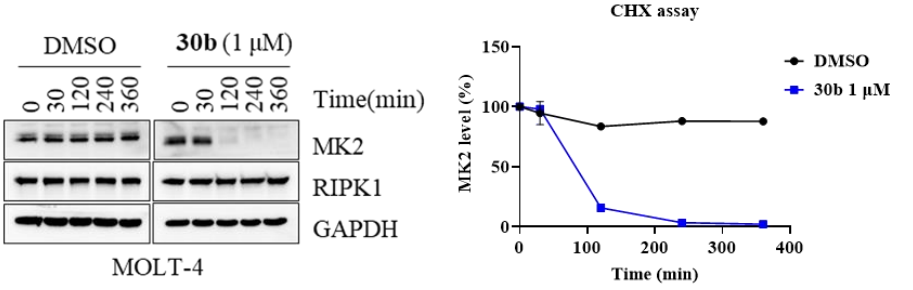

B

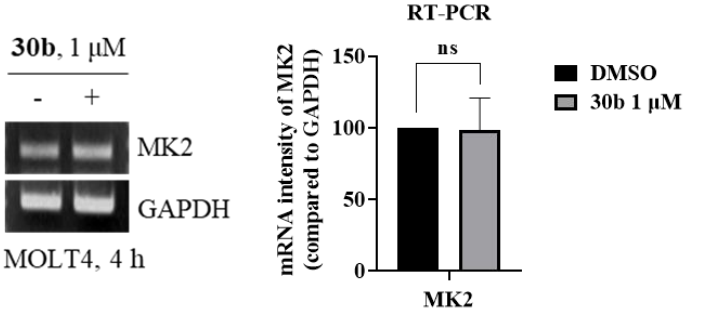

C

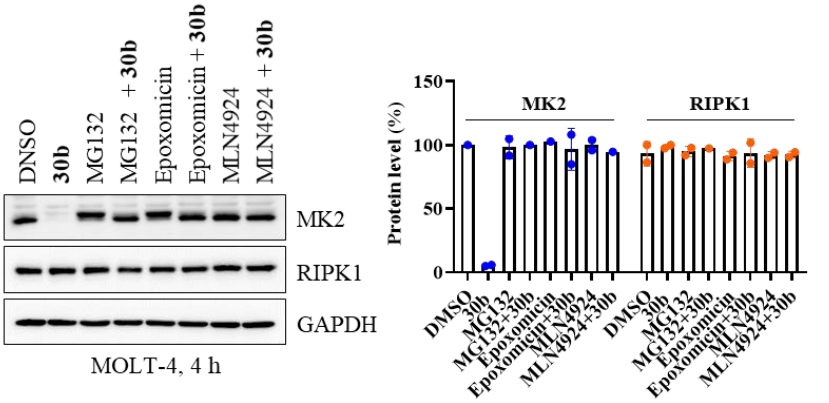

D

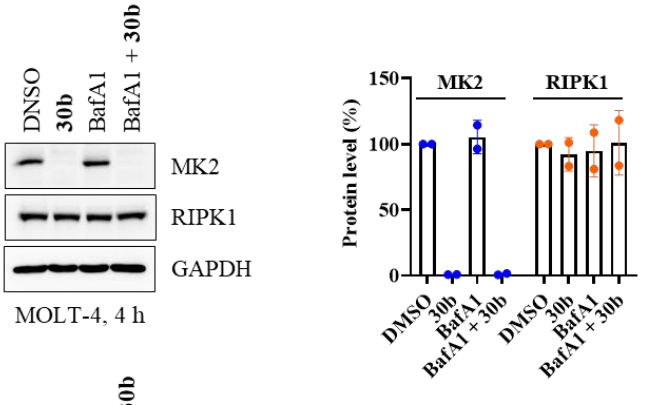

E

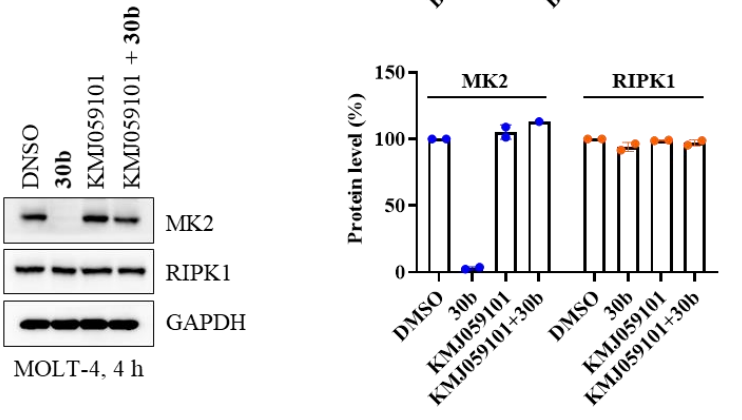

F

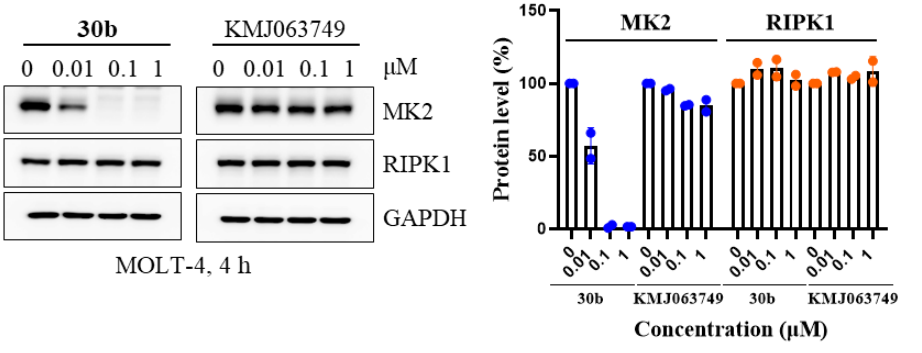

G

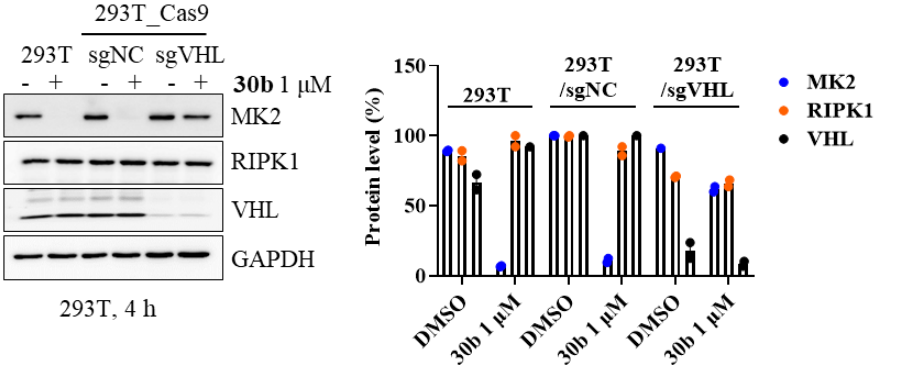

Figure 5. 30b degrades MK2 in UPS system by mediating VHL. (A) Cycloheximide (CHX) chase assay. MOLT-4 cells were pre-treated with 100 μg/ml CHX for 1 h prior to treating for the indicated times with either DMSO or **30b**. The right panel is a graphical representation of image quantification performed using image J. (B) RT-PCR was performed after 4 h treatment with either DMSO or **30b** in MOLT-4 cells. Statistical significance was calculated with "Student's" t-test analysis (NS: not significance) (C) Western blot analysis in MOLT-4 cells. The proteasome inhibitor MG132 (3 μM), Epoxomicin (3 μM) and the neddylation inhibitor MLN4924 (3 μM) were pre-treated for 1 h and subsequently treated with either DMSO or **30b** for 4 h. (D) Western blot analysis in MOLT-4 cells. The autophagolysosome inhibitor BafA1 (200 nM) was pretreated for 1 h and treated with DMSO and **30b** for 4 h. (E) Western blot analysis in MOLT-4 cells. Each warhead of **30b** were pre-treated for 1 h and then DMSO and **30b** for 4 h. (F) Western blot analysis in 293T cells. **30b** and KMJ063149 (negative control) were treated for 4 h. (G) Western blot analysis in 293T, 293T-Cas9-sgNC, and 293T-Cas9-sgVHL (VHL knockout cell), **30b** were treated for 4 h. All data shown in **Figure 5** were performed in duplicates and normalized to GAPDH. Western blot intensities were quantified using image J software and shown in the graph (right panel, average ± SD).

3. 30b interacts directly with VHL to induce a UPS system

To investigate the interaction between VHL and **30b,** we performed a target engagement assay using FACS, Operretta for imaging analysis and cellular thermal shift assay (CETSA).

We incubated BRD4 degrader MZ1 (1 μM) and **30b** degraders together for 4 h on BRD4-GFPΩmCherry HELA cells which expressed BRD4-GFP and mCherry (as a control) respectively. In the group treated with MZ1 alone, the GFP signal decreased by about 80% compared to DMSO group. In contrast, the experimental group that was treated with a combination of MZ1 showed an increase in the GFP signal in a concentration-dependent manner (10, 30, 50 μM) (**Figure 6A-6B**). Using the FACS, we demonstrated that **30b** occupies the binding site of VHL when its concentration increases by competing with MZ1. To capture the fluorescence images, we conducted Operretta using the same conditions as the FACS results. Consistent with previous evaluation (**Figure 6A-6B**), it was shown that in the combination treatment group, the GFP signal was restored like that of the DMSO group. (**Figure 6C**)

In addition, we conducted a cellular thermal shift assay (CETSA) to investigate how degraders interact with VHL and form complexes. This is because it has been observed that it directly binds to VHL. This investigation was completed using an assay that measures an increase in thermal resistance when the ligand and the corresponding protein bind. **Figure 6D-6E** indicated that **30b** treated group has more stability of MK2 than DMSO treated group. The collective findings show that **30b** is directly incorporated with VHL.

A

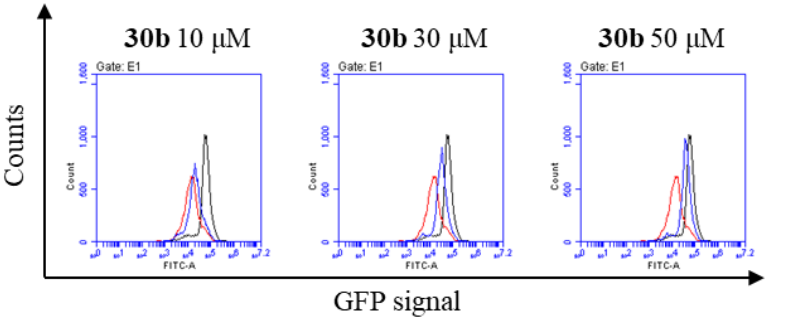

B

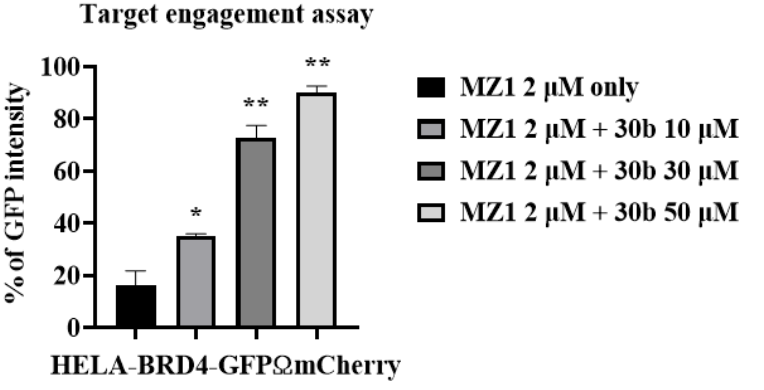

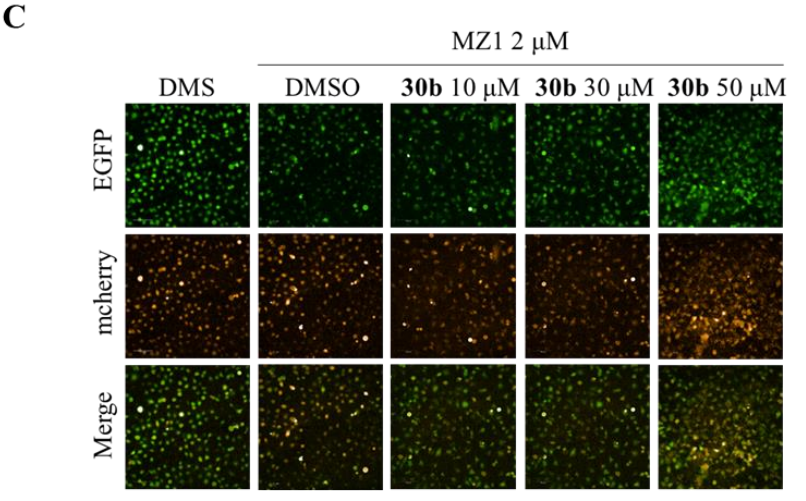

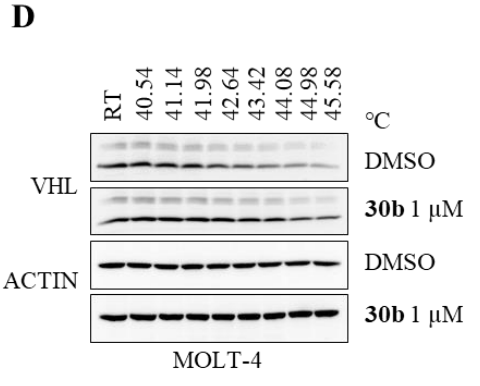

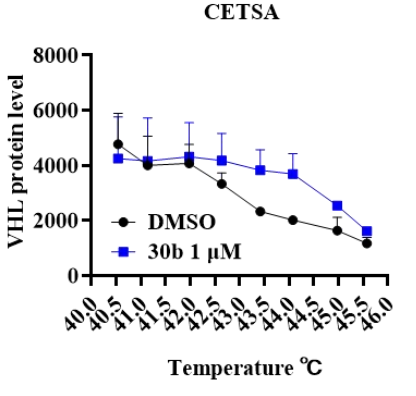

Figure 6. Investigation of VHL binding mode of 30b. (A-B) BRD4-GFP cell population was detected by flow cytometry analysis against BRD4-GFP mCherry HELA cell lines that express BRD4-GFP and mCherry simultaneously. Cells were treated with indicated analogue for 4 h. The colors of each FACS graph are as follows; red: MZ1, blue: **30b**, black: DMSO. The Bar Graph describes the BRD4 - GFP signal for each experiment groups (n = 2). Statistical analysis was performed using "Student's" t-test analysis (* $p < 0.05$, ** $p < 0.01$) (C) Representative confocal operetta images. BRD4-GFP mCherry HELA cell lines were treated with MZ1 1 μM and **30b** 10, 30, 50 μM for 4h. (D-E) Immunoblotting for CETSA assay (left panel) and quantitative analysis (right panel) of VHL in MG132 1 μM were pre-treated for 1 h and **30b** were treated for 30 min MOLT-4 cells. Cells were heated under the corresponding temperature for 10 min.

4. 30b is an MK2 indirect degrader that does not bind directly to MK2

Conventional PROTACs induced degradation by forming a ternary complex between the target and E3 ligase [28]. To explore whether **30b** is degraded by direct binding to MK2, we performed *in vitro* kinase assay. Contrary to our expectations, **30b** possesses no *in vitro* enzymatic potency for MK2 (**Table 6**). The enzymatic activity results displayed that it did not bind to MK2. Some studies have reported that MK2 exist heterodimer with the p38alpha in the resting cells [29, 30]. So, we additionally measured the enzymatic activity against p38alpha, and the results described that **30b** had excellent enzymatic inhibitory potency against p38alpha (IC_{50} = 2.48 nM for p38alpha) (**Table 6**). By conducting CETSA assay, **Figure 7A-7B** showed that the results consistent with the *in vitro* biochemical assay data were obtained in MOLT-4 cells.

Based on *in vitro* kinase assay and CETSA results, we speculated that the degradation of MK2 would affect the degradation of p38alpha. Therefore, we evaluated the degradation activity for p38alpha in **30b** harnessing immunoblot analysis in dose dependent manner. As shown in **Figure 7C**, **30b** degraded p38alpha with DC_{50} values of 0.040 μM**.** Furthermore, we observed the degradation of MK2 and p38alpha over time. **Figure 7D** showed that compound **30b** completely reduced MK2 protein level at 4 h. After that, it reduced p38alpha by approximately 80% at 24 h compared to 0 h. The results indicate that MK2 is first degraded by **30b**, and then by p38alpha.

To identify how p38alpha is degraded through the formation of a ternary complex p38alpha-**30b**-VHL, we generated plasmids that express p38alpha-Halo and Nluc-VHL. And we carried out the NanoBRET ternary complex formation assay. As a result, we found that **30b** posits the ternary complex with p38alpha and VHL (**Figure 7E-7F**). Moreover, Minjoo Ko carried out a molecular docking study to obtain structural insights into the binding mode of action for **30b**. The X-ray co-crystal structures p38alpha – MK2 heterodimer complex (p38alpha

(PDB: 6SFO [31]) and MK2 (PDB: 4TYH [32]) and VHL E3 ligase complex (VHL (PDB: 4WQO [33]), EloB, EloC, CuL2, and RBX (PDB: 5N4W [34])) was docked with the trifluoroethoxy residue of **30b** and the VHL ligand. This structural modeling described that the trifluoromethoxy warhead of **30b** binds to p38alpha in a p38alpha – MK2 heterodimer complex and VHL E3 ligase complex is close to MK2 (**Figure 8**). This *in silico* study suggests that MK2 degradation following p38alpha binding of **30b** is the proximity between the VHL E3 ligase complex and MK2.

When taken as a whole, these data revealed that compound **30b** selectively and favorably binds to the p38alpha and initiates degradation of MK2 first and following degradation of p38alpha. And it degrades p38alpha by forming ternary complex between p38alpha and VHL. Herein, it was revealed that **30b** is the MK2 indirect degrader.

Table 6. *in vitro* kinase assay against MK2 and p38alpha of **30b**

IC_{50} (nM)[1, 2]	
Kinase	**30b**
MK2	N.D.[3]
p38alpha	2.48

[1]*in vitro* biochemical kinase assay results.

[2]IC_{50} was measured by RBC.

[3]N.D. is not determined.

A

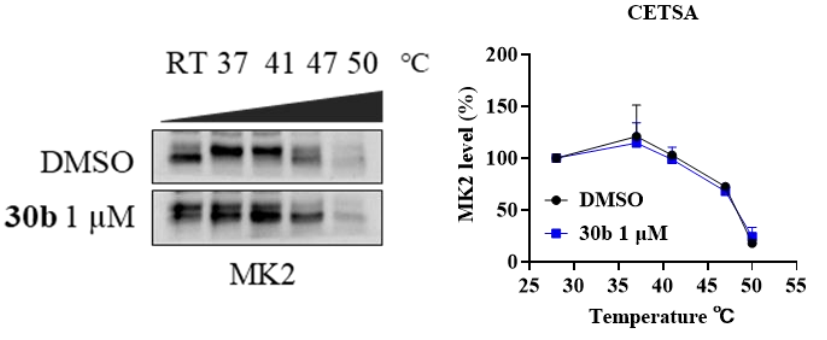

B

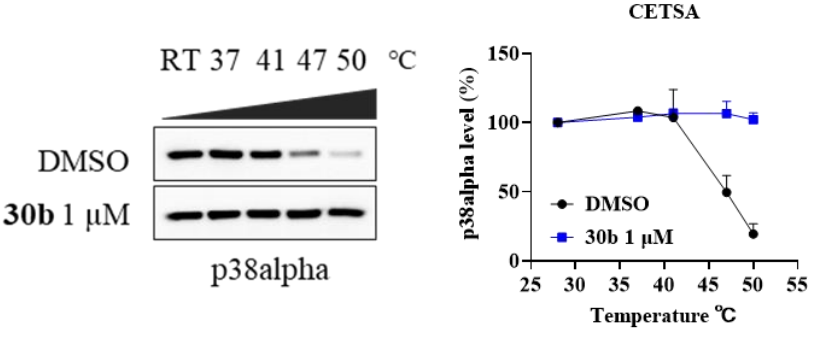

C

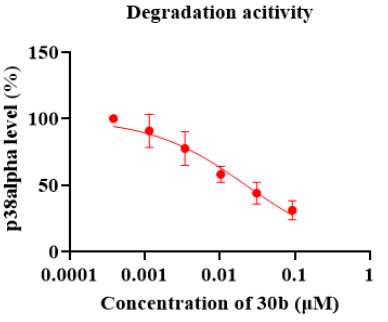

Compound	DC_{50} in MOLT-4 (μM)
	p38alpha
30b	0.040

D

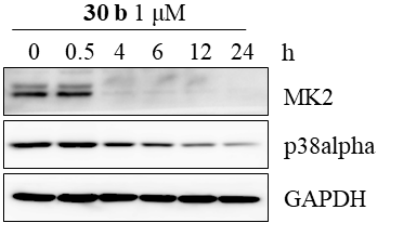

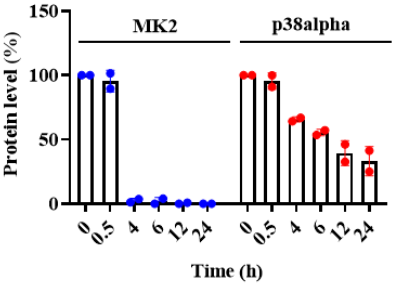

E

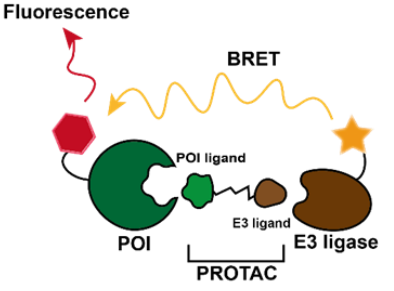

F

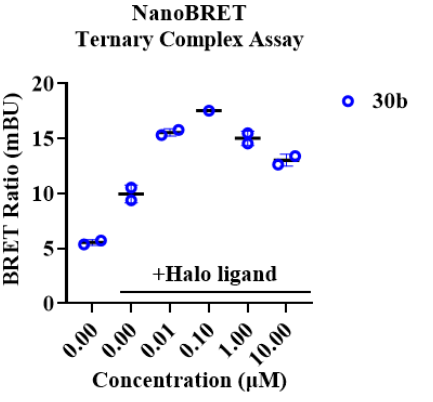

Figure 7. 30b is a degrader that directly binds to p38alpha and indirectly degrades MK2. (A-B) Evaluation of thermal stability for MK2 and p38alpha in MOLT-4 cells. A representative of two independent western blots of the heat stability of MK2 and p38alpha according to the indicated temperature when treated with DMSO and **30b**. Curve graphs were indicated immunoblot band were measured by image j (n = 2). (C) 50% protein degradation curve. Quantitative analysis was conducted using Image j (n = 2). (D) The indicated times, MOLT-4 cells were treated with **30b** (1 μM) and analyzed by western bolt analysis on their cell lysates. Quantitative results of western blot band intensity using Image J. The MK2/GAPDH ratios and p38alpha/GAPDH ratios were represented in the bar graph (n = 2). (E) The principle of the NanoBRET ternary complex assay was illustrated. (F) NanoBRET ternary complex formation of p38alpha. Co-transfected 293T cells which expressed both p38alpha-Halo and Nluc-VHL were treated with **30b** (1/10 serial dilution Max. 10 μM). Data displayed with average with standard deviation (n = 2, duplicate)

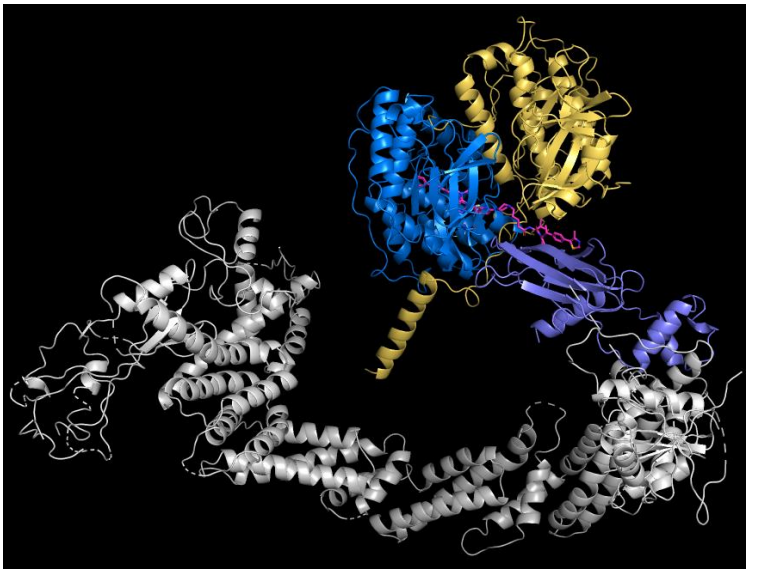

Figure 8. Molecular docking study of 30b conducted by Minjoo Ko. Predicted binding mode of **30b** in the p38alpha – MK2 heterodimer complex and E3 ligase complex. The calculation verification was performed by Namdoo Kim. The colors of this structure are respectively described below ; White: EloB, EloC, Cul2, RBX (PDB: 5N4W), Purple: VHL (PDB: 4WQO), Blue: p38alpha (PDB: 6SFO), Yellow: MK2 (PDB: 4TYH) Magenta: **30b**. All the X-ray co-crystal structures used in the docking study were copied from PDB website.

5. *in vivo* efficacy of 30b in a MOLT-4 mouse xenograft model

To figure out potential degradation effect of **30b** in MOLT-4 mouse xenograft model, first we established the mouse xenograft model bearing MOLT-4 cells. For this purpose, we injected $5x10^6$ cells/mouse into immunodeficient mice subcutabeously. When the tumor volume in each mouse became palpable (100 mm^3), mice were separated into two groups (n = 5) and administrated intravenously with either vehicle or 10 mg/kg/day **30b** twice a week for 3 weeks. We measured the tumor size and body weight by a caliper once every two days. Consistent with anti-proliferation observation in MOLT-4 (GI_{50} of **30b** = 6.51 μM) (**Figure 9A**), **30b** has moderate capacity of tumor growth inhibition in MOLT-4 mouse xenograft model. The average of tumor volume in group injected with vehicle and **30b** 10 mpk were 100% and 60% individually. And the body weight of the mice did not decrease during the period of drug administration (**Figure 9B-9D**). As a result, **30b** suggests that it is not toxic to mice and has a decent tumor growth inhibition.

Moreover, we performed *in vivo* western blot analysis to investigate the degradation level against MK2 and p38alpha in MOLT-4 mouse xenograft model. After 21 days of administration, we sacrificed the tumor tissue from the right flank of the mice. Subsequently, the tumor tissue was lysed with homogenizer and we conducted *in vivo* immunoblotting. As shown in **Figure 9E-9F,** in accordance with previous *in vitro* western blot data (**Figure 4D, Figure 7C)**. In **Figure 9E-9F**, MK2 level (% of degradation = 89%) was markedly diminished in MOLT-4 mouse xenograft model treated with **30b**. And a slight decrease of p38alpha (% of degradation = 28.9%) was observed. Collectively, all of these results indicate that compound **30b** effectively reduces MK2 level in *in vivo* model, which is consistent with *in vitro* studies.

A

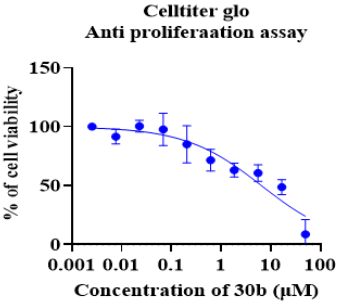

Compound	GI_{50} in MOLT-4 (μM)
30b	6.51

B

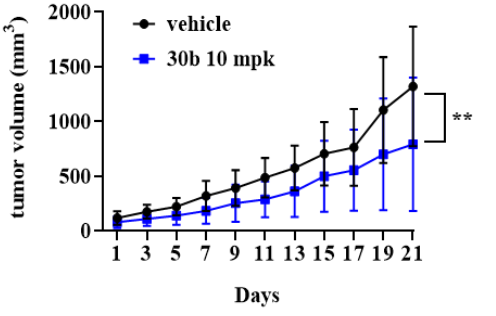

C

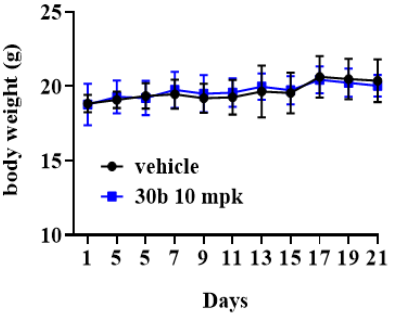

D

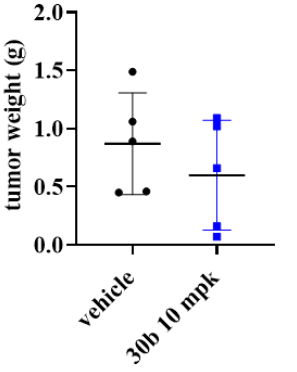

E

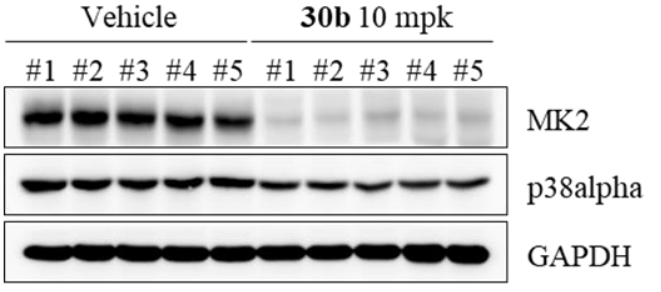

F

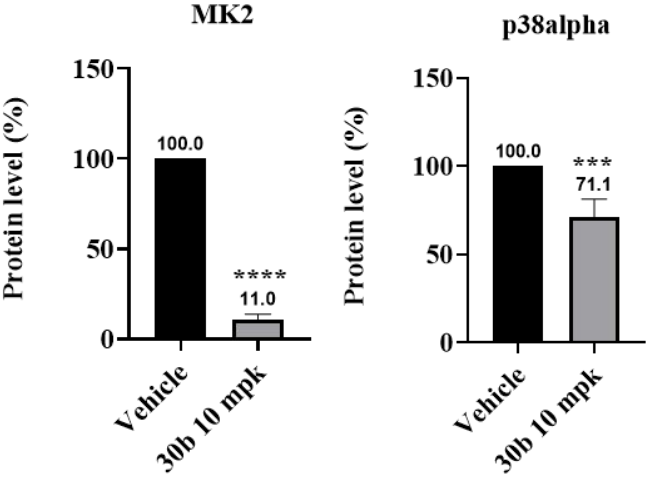

Figure 9. *in vivo* efficacy and degradation activity of MK2 and p38alpha in MOLT-4 mouse xenograft model. (A) Anti-proliferation assay of **30b**. MOLT-4 cells were incubated with serially diluted **30b** (1/3 serial dilution, Max. 50 μM) for 72 h. Viable cells were measured using the Cell titer-Glo solution (n = 3, duplicate). (B) Tumor growth curves. MOLT-4 tumour bearing immunodeficient mice were injected intravenously vehicle and 10 mpk **30b** twice a week for 21 days (n = 5, for each group). Tumor volume was calculated every two days for 21 days. Statistical analysis was conducted by "Student's" t-test (** $p < 0.01$). (C) Body weight curves. All body weight of MOLT-4 xenograft mouse model was measured every two days for 21 days. (D) Graph tumor mass. Following the extraction of the tumor tissue from the mice, the tumor mass was evaluated after 21 days. (E-F) *in vivo* western blot data and Bar graphs quantifying western bands (compared to vehicle and GAPDH). Statistical significance was performed by "Student's" t-test (*** $p < 0.001$, **** $p < 0.0001$). All data are showed as average with standard deviation.

IV. DISCUSSION

Many researchers have developed agents targeting kinases such as small molecule kinase inhibitors (SMKIs) [35]. But there are still limitations many SMKIs being effective in targeting disease-related "undruggable" kinases [36]. To overcome these challenges, recently, targeted protein degradation (TPD) technology has emerged [37]. This new strategy for undruggable targeting kinases that degrades targeted molecules by utilizing the intracellular degradation system including UPS system [38]. PROTAC (proteolysis targeting chimera) is the major type of TPD technology [39] [40]. Many laboratories are motivated by previously reported inhibitors to synthesize degraders for specific target kinases [41]. For an example, MZ1 is a BRD4 degrader that inspired from the BET inhibitor, JQ1 [42].

To best our knowledge, this study is the first structure activity relationship (SAR) study of PROTAC based MK2 degrader with GNF-7 moiety. GNF-7 is a promiscuous inhibitor targeting multi-kinase [43]. From our previous global proteomics profiling study for promiscuous VHL and CRBN degraders [13], we came up with effective approach how to synthesize and design for MK2-RIPK1 dual degraders. Based on previous global proteomics profiling approach, we synthesized 16 substances consisting of the multi-targeted inhibitor, GNF-7 and the E3 ligase binders (VHL and CRBN) by conjugating with linker. Through SAR study, we described that GNF-7 degraders with VHL (**18a**-**18b**, **18e**-**18g)** have more effective to degrade MK2 and RIPK1. And it was unveiled that degraders with linkers of more than 8 carbons have reduced degradation effect on MK2 and RIPK1. It was shown that the degraders of warhead modified with bulky residues (**27a-27c, 30b, 37a-37b, 42**) confers selectivity toward MK2. Based on previous report [44], the selectivity for ALK was increased when introducing an isopropoxy group to warhead, which is bulkier than the methoxy residue. Our SAR results also suggest that the bulkiest moiety, trifluoroethoxy induce the most selectivity for MK2 over RIPK1. Therefore, we selected **30b** introducing trifluoroethoxy warhead as a representative compound.

In this thesis, we identified novel MK2 indirect degrader, **30b** by *in vitro* kinase biochemical assay. We speculated that the degradation of MK2 might be related to p38alpha through the direct binding for **30b** to p38alpha. Because MK2 is the one of the downstream substrate of p38alpha [45, 46]. MK2 forms a heterodimer complex with p38alpha in the resting cells and upon activation p38alpha directly phosphorylates the MK2 [47, 48]. Co-crystal structure of complex with MK2 and p38alpha has been reported [29]. **30b** showed that the ternary complex formation between p38alpha and VHL was decreased not only in MK2 but also in p38alpha. And MK2 is decreased faster than p38alpha by **30b**. Through these results, we discussed the possibility that **30b** binds to p38alpha in p38alpha – MK2 heterodimer complex and VHL is closer to MK2 than p38alpha and degrades it first by ubiquitination. Minjoo ko conducted molecular docking study. This study described that **30b** binds into p38alpha – MK2 heterodimer complex and initiates an E3 complex that includes VHL with a distinctive spatial arrangement, the Lys-containing helix of MK2 pointing towards the E3 complex (**Figure 8**). However, in this thesis, we predicted that the MK2 degradation mechanism of **30b** was caused by p38alpha. In order to support our hypothesis more accurately, the co-crystal structure that MK2-p38alpha heterodimer complex with **30b** must be demonstrated. Therefore, it is necessary for in depth studies about MK2 degradation mechanism.

MAPKAPK2 (MK2) is the one of the potential therapeutic targets. MK2 is activated by p38alpha under external stimuli and phosphorylates RNA binding proteins (RBPs) and modulates mRNA expression related pro-inflammatory factors, cytokines, proto oncogene [49, 50, 51]. Hence, Some inhibitors targeting MK2 have been emerged and unveiled potency in inflammatory diseases (rheumatoid arthritis, psoriasis, inflammatory bowel disease) [52, 53, 54, 55, 56]. And also MK2 inhibition are associated with cancer cell progression such as multiple myeloma, head and neck cancer, gastrointestinal cancers [57, 58, 59]. However, the present MK2 inhibitors face significant drawbacks to develop clinical development due to limited solubility, low cell penetration, selectivity towards kinases, and

biochemical efficiency. ATI450 is the only compound entering phase 2 clinical trials currently. Therefore, development of various types of drugs such as PROTAC is necessary, MK2 degrader derived from this study will provide the valuable resource for development of MK2 targeted drugs in the further study. Moreover, we have also covered degraders for RIPK1 and MK2. RIPK1, which responds downstream of TNFR1, is a key mediator of inflammation. Many RIPK1 inhibitors such as Nec1, GSK772, DNL747 have developed for the treatments of human inflammatory diseases and neurodegenerative diseases [60, 61]. Therefore, it is believed that a degradation agent that degrades both MK2 and RIPK1 simultaneously will have a synergistic effect on various inflammatory diseases.

V. CONCLUSION

PROTAC (proteolysis-targeting chimera) technology based degrader is one of the most therapeutic modality. This hetero bifunctional molecule comprise protein of interest recognizing warhead, E3 ligase binding ligand and a linker joining the both ligands. The two ligands in PROATC protein degrader induce binding of target protein and E3 ligase. The target protein is ubiquitinated by E3 ligase and degraded by the intracellular proteasome system [62].

As part of a study aimed at providing global proteomics screening data set, we previously synthesized promiscuous warhead, GNF-7 based degraders. And we discovered GNF-7 based VHL degraders with degradation selectivity for MK2 and RIPK1. Based on our previous research, a SAR study was conducted to optimize GNF-7 moiety degraders. In this current effort, we designed and synthesized 16 GNF-7 warhead moiety analogues based on PROTAC. Through SAR study, we demonstrated MK2-RIPK1 degraders. Among them, **18e** showed most potent degradation activity both MK2 and RIPK1, MK2 DC_{50} = 0.003 μM, RIPK1 DC_{50} = 0.017 μM. Further, **30b** in which a bulky group, trifluoroexthoxy pyridine, was introduced into warhead observed high selectivity for MK2 over RIPK1 (DC_{50} values of MK2 = 0.005 ± 0.001 μM and RIPK1 = >2.5 μM).

Our degradation mechanism investigations have proved that the compound **30b** degraded MK2 by mediating VHL via ubiquitin proteasome system (UPS). Notably, **30b** potently suppressed p38alpha with IC_{50} values of 2.48 nM. Therefore, we also examined the degradation activity of p38alpha by compound **30b**. The results showed that **30b** has a poor degradation effect on p38alpha, unlike MK2. Furthermore, molecular docking study result indicated that **30b** forms ternary complex between p38alpha-MK2 complex and VHL. This finding supported our hypothesis that MK2 was degraded mediating p38alpha. Finally, by performing *in vivo* experiments, MK2 was almost completely reduced by 89% compared to vehicle by **30b** in the MOLT-4 mouse

xenograft model.

Taken together, our study suggests insightful guidelines for the design and development of MK2-RIPK1 dual degraders and MK2 selective degraders. And, we believe that this study contributes to improving development new drugs for MK2 related inflammatory and oncology disorders.

REFERENCES

1. Kanev GK, de Graaf C, de Esch IJP, Leurs R, Würdinger T, Westerman BA, et al. The Landscape of Atypical and Eukaryotic Protein Kinases. Trends in Pharmacological Sciences 2019;40:818-32.
2. Manning G, Whyte DB, Martinez R, Hunter T, Sudarsanam S. The Protein Kinase Complement of the Human Genome. Science 2002;298:1912-34.
3. Ayala-Aguilera CC, Valero T, Lorente-Macías Á, Baillache DJ, Croke S, Unciti-Broceta A. Small Molecule Kinase Inhibitor Drugs (1995–2021): Medical Indication, Pharmacology, and Synthesis. Journal of Medicinal Chemistry 2022;65:1047-131.
4. Coussens L, Parker PJ, Rhee L, Yang-Feng TL, Chen E, Waterfield MD, et al. Multiple, Distinct Forms of Bovine and Human Protein Kinase C Suggest Diversity in Cellular Signaling Pathways. Science 1986;233:859-66.
5. Bhullar KS, Lagarón NO, McGowan EM, Parmar I, Jha A, Hubbard BP, et al. Kinase-targeted cancer therapies: progress, challenges and future directions. Molecular Cancer 2018;17:48.
6. Attwood MM, Fabbro D, Sokolov AV, Knapp S, Schiöth HB. Trends in kinase drug discovery: targets, indications and inhibitor design. Nature Reviews Drug Discovery 2021;20:839-61.
7. Yu F, Cai M, Shao L, Zhang J. Targeting Protein Kinases Degradation by PROTACs. Frontiers in Chemistry 2021;9.
8. Cromm PM, Crews CM. Targeted Protein Degradation: from Chemical Biology to Drug Discovery. Cell Chemical Biology 2017;24:1181-90.
9. Adjei AA. What Is the Right Dose? The Elusive Optimal Biologic Dose in Phase I Clinical Trials. Journal of Clinical Oncology 2006;24:4054-5.
10. Qi S-M, Dong J, Xu Z-Y, Cheng X-D, Zhang W-D, Qin J-J. PROTAC: An Effective Targeted Protein Degradation Strategy for Cancer Therapy. Frontiers in Pharmacology 2021;12.
11. Pettersson M, Crews CM. PROteolysis TArgeting Chimeras (PROTACs) — Past, present and future. Drug Discovery Today: Technologies 2019;31:15-27.
12. Coleman KG, Crews CM. Proteolysis-Targeting Chimeras: Harnessing the Ubiquitin-Proteasome System to Induce Degradation of Specific Target Proteins. Annual Review of Cancer Biology 2018;2:41-58.
13. Donovan KA, Ferguson FM, Bushman JW, Eleuteri NA, Bhunia D,

Ryu S, et al. Mapping the Degradable Kinome Provides a Resource for Expedited Degrader Development. Cell 2020;183:1714-31.e10.
14. Gaestel M. MAPK-Activated Protein Kinases (MKs): Novel Insights and Challenges. Frontiers in cell and developmental biology 2016;3.
15. White A, Pargellis CA, Studts JM, Werneburg BG, Farmer BT. Molecular basis of MAPK-activated protein kinase 2:p38 assembly. Proceedings of the National Academy of Sciences 2007;104:6353-8.
16. Soni S, Anand P, Padwad YS. MAPKAPK2: the master regulator of RNA-binding proteins modulates transcript stability and tumor progression. Journal of Experimental & Clinical Cancer Research 2019;38:121.
17. Hitti E, Iakovleva T, Brook M, Deppenmeier S, Gruber AD, Radzioch D, et al. Mitogen-Activated Protein Kinase-Activated Protein Kinase 2 Regulates Tumor Necrosis Factor mRNA Stability and Translation Mainly by Altering Tristetraprolin Expression, Stability, and Binding to Adenine/Uridine-Rich Element. Molecular and Cellular Biology 2006;26:2399-407.
18. Kotlyarov A, Neininger A, Schubert C, Eckert R, Birchmeier C, Volk H-D, et al. MAPKAP kinase 2 is essential for LPS-induced TNF-α biosynthesis. Nature Cell Biology 1999;1:94-7.
19. Neininger A, Kontoyiannis D, Kotlyarov A, Winzen R, Eckert R, Volk H-D, et al. MK2 Targets AU-rich Elements and Regulates Biosynthesis of Tumor Necrosis Factor and Interleukin-6 Independently at Different Post-transcriptional Levels*. Journal of Biological Chemistry 2002;277:3065-8.
20. Newman R, McHugh J, Turner M. RNA binding proteins as regulators of immune cell biology. Clinical and Experimental Immunology 2015;183:37-49.
21. Duraisamy S, Bajpai M, Bughani U, Dastidar SG, Ray A, Chopra P. MK2: a novel molecular target for anti-inflammatory therapy. Expert Opinion on Therapeutic Targets 2008;12:921-36.
22. Gaur R, Mensah KA, Stricker J, Adams M, Parton A, Cedzik D, et al. CC-99677, a novel, oral, selective covalent MK2 inhibitor, sustainably reduces pro-inflammatory cytokine production. Arthritis Research & Therapy 2022;24:199.
23. Gordon D, Hellriegel ET, Hope HR, Burt D, Monahan JB. Safety, Tolerability, Pharmacokinetics, and Pharmacodynamics of the MK2 Inhibitor ATI-450 in Healthy Subjects: A Placebo-Controlled, Randomized Phase 1 Study. Clinical Pharmacology: Advances and Applications 2021;13:123-34.
24. Fiore M, Forli S, Manetti F. Targeting Mitogen-Activated Protein

Kinase-Activated Protein Kinase 2 (MAPKAPK2, MK2): Medicinal Chemistry Efforts To Lead Small Molecule Inhibitors to Clinical Trials. Journal of Medicinal Chemistry 2016;59:3609-34.
25. Hope HR, Hockerman S, Saabye M, Stillwell L, Basavalingappa R, Emanual C, et al. ATI-450: A Novel MK2 Pathway Inhibitor - Preclinical & Clinical Translational Studies to Predict Human Dose. Journal of Pharmacology and Experimental Therapeutics 2023;385:231.
26. Tran QTN, Gan PXL, Liao W, Mok YK, Chai CLL, Wong WSF. Degradation of MK2 with natural compound andrographolide: A new modality for anti-inflammatory therapy. Pharmacological Research 2023;194:106861.
27. Ding W-X, Yin X-M. Sorting, recognition and activation of the misfolded protein degradation pathways through macroautophagy and the proteasome. Autophagy 2008;4:141-50.
28. Grigglestone CE, Yeung K-S. Degradation of Protein Kinases: Ternary Complex, Cooperativity, and Selectivity. ACS Medicinal Chemistry Letters 2021;12:1629-32.
29. Haar Et, Prabakhar P, Liu X, Lepre C. Crystal Structure of the P38α-MAPKAP Kinase 2 Heterodimer*. Journal of Biological Chemistry 2007;282:9733-9.
30. Gomez-Gutierrez P, Campos PM, Vega M, Perez JJ. Identification of a Novel Inhibitory Allosteric Site in p38α. PLOS ONE 2016;11:e0167379.
31. Röhm S, Berger B-T, Schröder M, Chaikuad A, Winkel R, Hekking KFW, et al. Fast Iterative Synthetic Approach toward Identification of Novel Highly Selective p38 MAP Kinase Inhibitors. Journal of Medicinal Chemistry 2019;62:10757-82.
32. Cumming JG, Debreczeni JÉ, Edfeldt F, Evertsson E, Harrison M, Holdgate GA, et al. Discovery and Characterization of MAPK-activated Protein Kinase-2 Prevention of Activation Inhibitors. Journal of Medicinal Chemistry 2015;58:278-93.
33. Nguyen Henry C, Yang H, Fribourgh Jennifer L, Wolfe Leslie S, Xiong Y. Insights into Cullin-RING E3 Ubiquitin Ligase Recruitment: Structure of the VHL-EloBC-Cul2 Complex. Structure 2015;23:441-9.
34. Cardote TAF, Gadd MS, Ciulli A. Crystal Structure of the Cul2-Rbx1-EloBC-VHL Ubiquitin Ligase Complex. Structure 2017;25:901-11.e3.
35. Lightfoot HL, Goldberg FW, Sedelmeier J. Evolution of Small Molecule Kinase Drugs. ACS Medicinal Chemistry Letters 2019;10:153-60.

36. Zhong L, Li Y, Xiong L, Wang W, Wu M, Yuan T, et al. Small molecules in targeted cancer therapy: advances, challenges, and future perspectives. Signal Transduction and Targeted Therapy 2021;6:201.
37. Sakamoto KM, Kim KB, Kumagai A, Mercurio F, Crews CM, Deshaies RJ. Protacs: Chimeric molecules that target proteins to the Skp1–Cullin–F box complex for ubiquitination and degradation. Proceedings of the National Academy of Sciences 2001;98:8554-9.
38. Zhao L, Zhao J, Zhong K, Tong A, Jia D. Targeted protein degradation: mechanisms, strategies and application. Signal Transduction and Targeted Therapy 2022;7:113.
39. Sakamoto KM, Kim KB, Kumagai A, Mercurio F, Crews CM, Deshaies RJ. Protacs: Chimeric molecules that target proteins to the Skp1-Cullin-F box complex for ubiquitination and degradation. Proceedings of the National Academy of Sciences of the United States of America 2001;98:8554-9.
40. Li X, Song Y. Proteolysis-targeting chimera (PROTAC) for targeted protein degradation and cancer therapy. Journal of Hematology & Oncology 2020;13:50.
41. Benowitz AB, Jones KL, Harling JD. The therapeutic potential of PROTACs. Expert Opin Ther Pat 2021;31:1-24.
42. Zengerle M, Chan K-H, Ciulli A. Selective Small Molecule Induced Degradation of the BET Bromodomain Protein BRD4. ACS Chemical Biology 2015;10:1770-7.
43. Choi HG, Ren P, Adrian F, Sun F, Lee HS, Wang X, et al. A Type-II Kinase Inhibitor Capable of Inhibiting the T315I "Gatekeeper" Mutant of Bcr-Abl. Journal of Medicinal Chemistry 2010;53:5439-48.
44. Marsilje TH, Pei W, Chen B, Lu W, Uno T, Jin Y, et al. Synthesis, Structure–Activity Relationships, and in Vivo Efficacy of the Novel Potent and Selective Anaplastic Lymphoma Kinase (ALK) Inhibitor 5-Chloro-N2-(2-isopropoxy-5-methyl-4-(piperidin-4-yl)phenyl)-N4-(2-(isopropylsulfonyl)phenyl)pyrimidine-2,4-diamine (LDK378) Currently in Phase 1 and Phase 2 Clinical Trials. Journal of Medicinal Chemistry 2013;56:5675-90.
45. Stokoe D, Campbell DG, Nakielny S, Hidaka H, Leevers SJ, Marshall C, et al. MAPKAP kinase-2; a novel protein kinase activated by mitogen-activated protein kinase. The EMBO Journal 1992;11:3985-94.
46. Kumar S, Boehm J, Lee JC. p38 MAP kinases: key signalling molecules as therapeutic targets for inflammatory diseases. Nature

Reviews Drug Discovery 2003;2:717-26.
47. Lukas SM, Kroe RR, Wildeson J, Peet GW, Frego L, Davidson W, et al. Catalysis and Function of the p38α·MK2a Signaling Complex. Biochemistry 2004;43:9950-60.
48. Ben-Levy R, Hooper S, Wilson R, Paterson HF, Marshall CJ. Nuclear export of the stress-activated protein kinase p38 mediated by its substrate MAPKAP kinase-2. Current Biology 1998;8:1049-57.
49. Gurgis FMS, Ziaziaris W, Munoz L. Mitogen-Activated Protein Kinase–Activated Protein Kinase 2 in Neuroinflammation, Heat Shock Protein 27 Phosphorylation, and Cell Cycle: Role and Targeting. Molecular Pharmacology 2014;85:345-56.
50. Winzen R, Kracht M, Ritter B, Wilhelm A, Chen C-YA, Shyu A-B, et al. The p38 MAP kinase pathway signals for cytokine-induced mRNA stabilization via MAP kinase-activated protein kinase 2 and an AU-rich region-targeted mechanism. The EMBO Journal 1999;18:4969-80.
51. Pereira B, Billaud M, Almeida R. RNA-Binding Proteins in Cancer: Old Players and New Actors. Trends in Cancer 2017;3:506-28.
52. Anderson DR, Meyers MJ, Kurumbail RG, Caspers N, Poda GI, Long SA, et al. Benzothiophene inhibitors of MK2. Part 2: Improvements in kinase selectivity and cell potency. Bioorganic & Medicinal Chemistry Letters 2009;19:4882-4.
53. Velcicky J, Feifel R, Hawtin S, Heng R, Huppertz C, Koch G, et al. Novel 3-aminopyrazole inhibitors of MK-2 discovered by scaffold hopping strategy. Bioorganic & Medicinal Chemistry Letters 2010;20:1293-7.
54. Schlapbach A, Feifel R, Hawtin S, Heng R, Koch G, Moebitz H, et al. Pyrrolo-pyrimidones: A novel class of MK2 inhibitors with potent cellular activity. Bioorganic & Medicinal Chemistry Letters 2008;18:6142-6.
55. Malona J, Chuaqui C, Seletsky BM, Beebe L, Cantin S, Kalken DV, et al. Discovery of CC-99677, a selective targeted covalent MAPKAPK2 (MK2) inhibitor for autoimmune disorders. Translational Research 2022;249:49-73.
56. Ray AL, Castillo EF, Morris KT, Nofchissey RA, Weston LL, Samedi VG, et al. Blockade of MK2 is protective in inflammation-associated colorectal cancer development. International Journal of Cancer 2016;138:770-5.
57. Guo M, Sun D, Fan Z, Yuan Y, Shao M, Hou J, et al. Targeting MK2 Is a Novel Approach to Interfere in Multiple Myeloma. Frontiers in oncology 2019;9.

58. Berggren KL, Restrepo Cruz S, Hixon MD, Cowan AT, Keysar SB, Craig S, et al. MAPKAPK2 (MK2) inhibition mediates radiation-induced inflammatory cytokine production and tumor growth in head and neck squamous cell carcinoma. Oncogene 2019;38:7329-41.
59. Jacenik D, Lebish EJ, Beswick EJ. MK2 drives progression of pancreas and colon cancers by suppressing CD8+ T cell cytotoxic function and is a potential immunotherapy target. Frontiers in Immunology 2023;14.
60. Mifflin L, Ofengeim D, Yuan J. Receptor-interacting protein kinase 1 (RIPK1) as a therapeutic target. Nature reviews Drug discovery 2020;19:553-71.
61. Degterev A, Ofengeim D, Yuan J. Targeting RIPK1 for the treatment of human diseases. Proceedings of the National Academy of Sciences 2019;116:9714-22.
62. Bhole RP, Kute PR, Chikhale RV, Bonde CG, Pant A, Gurav SS. Unlocking the potential of PROTACs: A comprehensive review of protein degradation strategies in disease therapy. Bioorganic Chemistry 2023;139:106720.

ABSTRACT (IN KOREAN)

신규한 MK2-RIPK1 이중 분해제의 생물학적 평가와 작용기전 연구

<지도교수 심태보>

연세대학교 대학원 의과학과

이지원

카이네이즈는 ATP의 gamma phosphate를 기질 단백질에 전달을 촉매 하는 효소이며 세포 내 신호전달에 핵심 역할을 한다. 이러한 특징으로 다양한 세포 신호 전달을 하고 세포 주기, 증식, 생장, 분화, 대사 및 염증을 포함한 세포 기능을 조절을 한다. 따라서 암, 면역 질환과 신경 질환을 포함한 많은 인간 질병을 유발과 관련이 깊은 것으로 알려져 있다. 이러한 이유로 비정상적인 기능을 하는 kinase를 저해하는 저분자 화합물이 개발되어 왔다. 하지만 약물 저항성, 선택성 부여와 undruggable 카이네이즈 공략 어려움과 같은 한계점이 존재한다. 따라서 신규한 약물 개발 연구가 필요하다.

최근에는 세포 내 단백질 분해 시스템을 활용한 약물 개발 플랫폼인 표적 단백질 분해 기법이 등장했다. 프로탁은 주요 표적 단백질 분해 기법 중 하나로 E3 ligase의 리간드와 표적단백질의 리간드가 연결체를 통해 연결된 이종이기능성 화합물이다. 프로탁은 E3 ligase와 표적 단백질 간의 삼중 복합체 형성을 한다. 이후 E3 ligase에 의해 유비퀴틴화된 표적 단백질을 세포 내 분해 시스템 중 하나인 프로테아좀에 의해 분해한다. 선행연구에서 GNF-7 매개 프로탁 기반 분해제들에 대하여 global proteomics screening을 진행하였다. 이를 통해 GNF-7 매개 VHL-분해제가 CRBN-분해제 대비 MK2와 RIPK1에 대한 분해 선택성이 있음을 확인하였다.

본 학위논문에서는 선행 연구 결과를 기반으로 구조 활성 연구 와 생물학적 평가 및 분해작용기전 연구를 진행하였고, 대표 화합물인 MK2 선택적 분해제, **30b**를 도출하였다. 먼저, GNF-7 골격을 보유한 16 종의 유도체에 대하여 MK2와 RIPK1에 대한 분해능 기반 구조 활성 평가를 진행하였다. GNF-7 골격에서 bulky한 잔기로 변형한 유도체들에서 MK2에 대한 분해 선택성이 우수하였다. 유도체들 중 대표 화합물 **30b**는 RIPK1 (DC_{50} = >2.5 μM) 대비 MK2 (DC_{50} = 0.005 ± 0.001 μM)에 대한 분해 선택성이 500 배 증가함을 보였다. 더 나아가 다양한 생물학적 평가 기법을 활용하여 **30b**에 대한 분해 기전을 규명하였다. 그 결과, **30b**는 MK2를 VHL을 매개하여 유비퀴틴 - 프로테아좀 시스템을 통한 간접 분해제임을 보여주었다. 생물학적 방법과 분자 도킹 연구를 바탕으로 p38alpha와의 직접 결합이 MK2 분해에 영향을 미칠 가능성을 예측하였다. 마지막으로 MOLT-4 종양 마우스 모델에서 준수한 종양 형성 억제능을 관찰하였고, 세포 수준의 분해 효과와 상응하는 분해능을 보였다.

표적 단백질인 MK2는 다양한 염증 신호 전달과 종양 형성 관련 유전자 발현을 조절하는 세포 내 주요 분자로 암과 염증을 유발하는 주요 원인이다. 이에 따라 MK2를 표적하는 저해제 개발이 되어 왔다. 하지만 타겟 선택성 부여와 같은 한계점에 직면하고 있다. 이를 극복하기 위해 간접 저해와 같은 다양한 전략이 제시되어왔다. 현재까지 PROTAC 기반의 MK2 분해제는 보고된 바가 없다. 종합하여, 본 학위 논문은 MK2에 대한 분해제 개발에 대한 통찰력을 제공할 수 있음을 시사한다. 또한 염증 질환과 암에 대한 적응증 확장 가능성을 보여준다.

핵심되는 말 : 카이네이즈, 표적 단백질 분해 기법, 프로탁, MK2, RIPK1, 유비퀴틴-프로테아좀 시스템, MK2-RIPK1 이중 분해제, MK2 선택적 분해제